How to map the resilience of hydrothermal vent fields: a tutorial

# Cross-ministerial Strategic Innovation Promotion Program

SIP

The Strategic Innovation Promotion Program (SIP) was launched by the Council for Science, Technology, and Innovation (CSTI), which oversees projects that target scientific and technological innovation in line with Japanese government directions as stated in the Comprehensive Strategy on Science Technology and Innovation and the Japan Revitalization Strategy. This interdisciplinary program among government agencies, academic institutes and private sectors addresses eleven issues. One of these issues is Next-Generation Technology for Ocean Resources Exploration.

Zipangu in the Ocean Program and Protocols for Environmental Survey Technologies

Zipangu in the Ocean Program is a technical study of the development of submarine mineral deposits that takes into consideration the wise use of these resources.

One research area is the ecological survey of organisms and their long-term monitoring. However, an ecosystem consists of various interrelated factors; thus, in addition to a comprehensive understanding of the system, observation and analysis of each component to its most elemental level are unavoidable. Recently, increased environmental awareness and the necessity of forming a consensus have become key issues in conducting development activities. Growing concern for the environment by the public and the diversification of the use of maritime areas have complicated the interests of stakeholders. To facilitate the formation of a consensus under these conditions, it is important for standardized methods to be implemented. This will ensure that research processes are transparent and that the collection of survey data is objective.

This protocol series aims to introduce more accurate, user-friendly, objective and effective underlying technologies required to understand the environmental impact of submarine mineral resource development. We believe that creating such a technology tool-kit will allow us to develop these resources in a sustainable manner.

○ Thermal activity   ● Cobalt-rich crust   ● REY-rich mud   ※1 based on *Usui et.al(1994)*
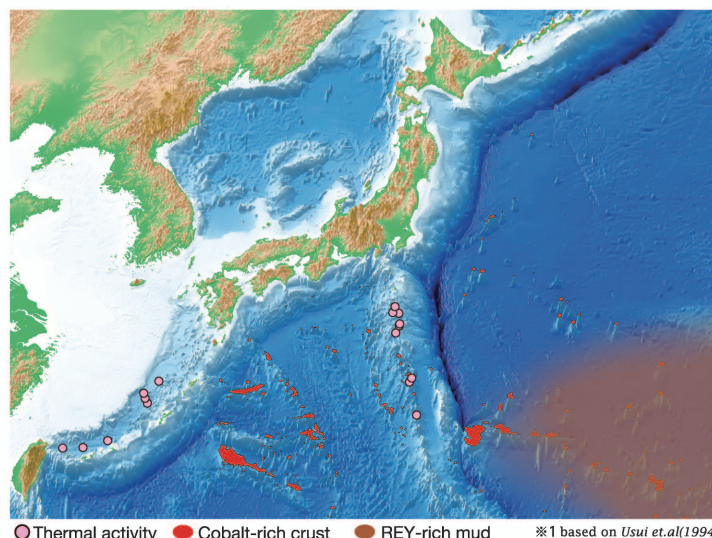
Table of Contents

Introduction

1.1. Potential impact of mining activities on deep-sea chemosynthetic communities

One of the targets for commercial mining is the Seafloor Massive Sulfides (SMSs) deposits formed around hydrothermal vents, which is a highly attractive source of copper, zinc, lead, gold and silver ores (Hoagland 2010, Herzig 1999, Binns and Scott 1993, Halbach et al. 1989). Hydrothermal vents host chemosynthetic communities as well as metal rich ores. The chemosynthetic communities consist of many endemic invertebrate species specifically adapted to the vent environment via microbial chemoautotrophic primary production (Van Dover 2010). These species have provided new scientific insights into the mechanisms by which organisms adopt to the extreme environment (Jannasch and Wirsen 1979). Furthermore, as reviewed by Le et al. (2016), ecological function and services of these communities range from providing habitat and refuge for other species including non-endemic species (Levin et al. 2016, Govenar 2010), playing a key role in global carbon, sulfur and heavy metals cycling (Jeanthon, 2000, D'Arcy and Amend 2013) and offering new biomolecules that could contribute to industrial development (Terpe et al. 2013, Mahon et al. 2015).

Mining of seafloor massive sulfide deposits potentially changes the physico-chemical environment of a vent community through the loss of sulfide habitat, degradation of sulfide habitat quality, modification of fluid flux regimes and exposure of surrounding seafloor habitats (including non-sulfide habitats) to sedimentation and heavy metal deposition (International Seabed Authority 2007, Van Dover 2014). This will directly affect the ecological community by removing and reclaiming organisms, reducing the amount of habitable substrate and changing resource supply. Physico-chemical models and organism distribution data have been integrated to estimate the potential area of sedimentation (Coffey Natural Systems 2008b). However, after the instantaneous effects of a disturbance, the ecological community will reach a new equilibrium state within the disturbed environment (Ives and Carpenter 2007). Hence, potential impacts of artificial disturbances, including how they may cause extinction and modify community structure at different spatial scales (local, regional and global), and decrease diversity at different biological levels (genetic, species and phylogenetic), will be understood by considering both direct impacts of mining activities and subsequent ecological responses. Environmental impact assessments (EIAs) that lack this point of view might severely underestimate the potential risks of anthropological activities.

1.2. Dispersal

Vent ecosystems are typically dominated by benthic invertebrate taxa (e.g., *Bathymodiolus* mussels, *Shinkaia* squat lobsters and *Alviniconcha* gastropods in Northwestern Pacific [Watanabe et al. 2010, Desbruyères et al. 2006. Podowski et al. 2010]) that host symbiotic, chemoautotrophic microorganisms. Deep-sea vents are known as ephemeral habitat islands from the moment of their discovery (Macdonald et al.,1980, Van Dover 2014), i.e, sustaining regional metacommunities nested within several biogeographic provinces linked by pelagic larval dispersal (Lutz et al. 1984). The frequency of disruptive natural disturbances to vent communities can range from several decades to several hundred years depending on the geological background of vent fields. Faunal adaptations for colonizing new vent fields are important aspects of the sustainability of these communities, especially since neighboring vent fields are often separated by 10s or 100s of kilometers. Vent-restricted taxa are often characterized by rapid growth rates, early maturation, large reproductive output, and well developed dispersal capabilities (Grassle, 1986). These characteristics are shared by opportunistic marine invertebrate species that persist despite frequent local extinctions and are divergent from those of deep-sea species in low-disturbance regimes (Grassle and

Sanders,1973, Van Dover 2014).

1.3. Resilience of vent ecosystems

Recoverability, or resilience, refers to persistence of ecosystems in the face of natural or anthropogenic disturbances (Holling 1973; Box 1). Resilience of vent communities indicates whether they are vulnerable or robust to natural disturbances, such as volcanic activity, and anthropogenic disturbances, such as mineral resource mining.

Box 1. What is resilience?

The concept of resilience in ecological systems was first introduced by C.S. Holling to describe the persistence of natural systems in the face of changes in ecosystem variables due to natural or anthropogenic causes (Holling 1973). In this document we defined resilience as **the time required for an ecosystem to return to an equilibrium or steady-state following a perturbation (Fig. B1a)**. This definition of resilience has been termed *engineering resilience* (Holling 1996). It is worth mentioning that there is another definition of resilience (*ecological resilience*) accounting for the capacity of a system to absorb disturbance and reorganize while undergoing change so as to still retain essentially the same function, structure, identity, and feedbacks *(Fig. B1b)*.
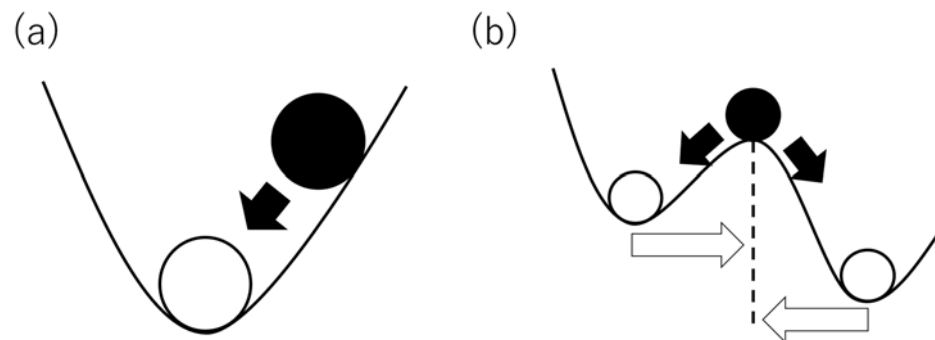

Figure B1. Illustrated example of *engineering resilience* (a) and *ecological resilience* (b). White circles indicate the stable states, black circles indicate states after disturbance, black arrows indicate the direction of change and white arrows indicate distance to a tipping point indicated by a dashed line.

Recently, Suzuki et al. (2018) introduced a model-based approach to determine the resilience of vent communities by integrating a meta-population model and the estimated larval dispersal between hydrothermal vent fields (HVFs). The key idea was to estimate resilience in terms of connectivity of vent communities through larval dispersal (Fig. 1). By simulating disturbances to vent fields, Suzuki et al. (2018) mapped recovery time of communities in 131 hydrothermal vent fields in the western Pacific Ocean. The purpose of this document is to show how this model can be used to optimize resource mining and provide a step-by-step tutorial for the readers who want to apply the methodology to their own data set.
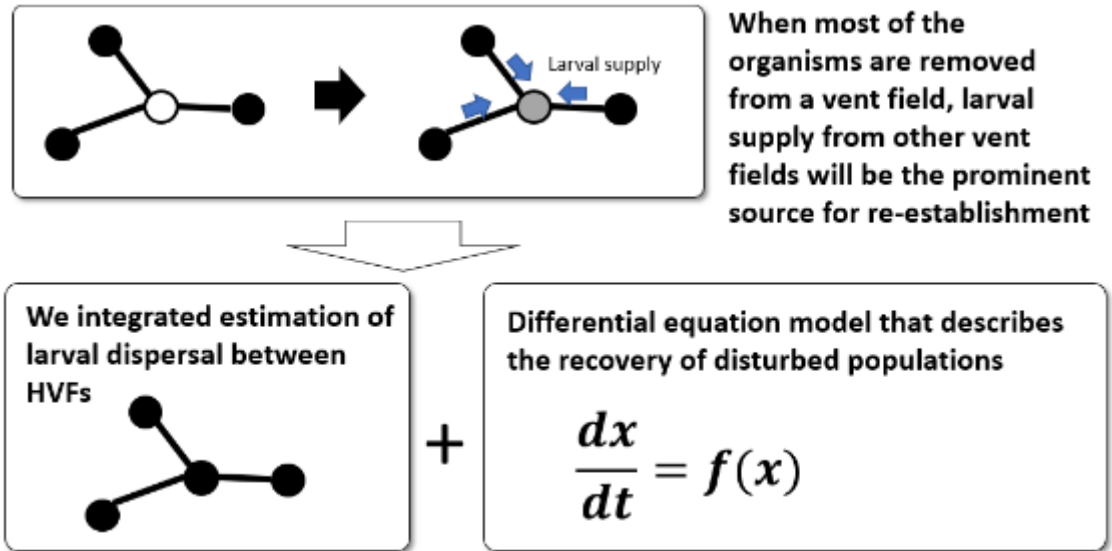
Figure 1. A schematic description of our approach.

Technical background

2.1. Dispersal matrix

A dispersal matrix $A = \{A_{ij}\}$ for the group of focal HVFs (or other distinct spatial units) must be prepared before starting the analysis. Here, A_{ij} is the dispersal rate that a larva produced at vent field j will migrate into *i* per unit time (e.g., year) and A_{ii} corresponds to self-recruitment. In the following analysis, we used the estimated larval dispersal between seven HVFs in Okinawa Trough (Iheya Ridge, Irabu Knoll, Izena Cauldron, Natsushima 84-1 Knoll, North Knoll Iheya Ridge, Dai-Yon Yonaguni Knoll and Hatoma Knoll) obtained from Mitarai et al. (2016). The results of Mitarai et al. (2016) were based on a unified model that accounts for the temperature dependence of larval development in marine animals (O'Connor et al. 2007) as well as a physical model describing deep-ocean circulation. Dispersal distance will depend both on the speed of ocean currents and expected duration of larvae at a given depth. For example, larvae that use shallower depths can disperse further because of fast ocean currents, although duration of the pelagic larval stage would be shortened when water temperature is higher (O'Connor et al. 2007).

In addition to the bio-physical approach, our method is also applicable to the dispersal matrix estimated from spatial genetic diversity (Beerli and Palczewski 2010, Chen et al. 2015). Using the dispersal matrix of a galatheid crab, *Shinkaia crosnieri*, in Okinawa Trough (Watanabe et al. unpublished data), Suzuki et al. (2018) found some consistency in estimated recovery time both from the dispersal matrix estimated by the bio-physical model (Mitarai et al. 2016) and the matrix estimated from genetic diversity.

2.2. Model

We used a differential equation for our analysis, which is described as,

$$\frac{dx_i}{dt} = f_i(x_i). \qquad (1)$$

Generally, a differential equation describes the time evolution of the variable x_i (here, it represents population size of organisms in HVF *i* based on some processes implemented as a mathematical representation in function f_i. Specifically, we used the following function,

$$f_i(x_i) = \left(1 - \frac{x_i}{K_i}\right)\left(rA_{ii}x_i + r\sum_{j\neq i}A_{ji}K_j\right). \qquad (2)$$

Here, K_i is the carrying capacity (equilibrium population size of vent field *i*), r is the reproduction

rate defined as the number of larvae that one individual produces per year and A_{ij} is the dispersal rate that a larva produced at vent field j will migrate into i per year, where A_{ii} corresponds to self-recruitment. The dispersal networks were implemented as a dispersal matrix A whose elements are A_{ii} and A_{ij}. In equation (1,2),

$$rA_{ii}x_i,$$

represents the recruitment of larvae from the HVF i and,

$$r\sum_{j\neq i}A_{ji}K_j,$$

represents the recruitment of individuals from other vent fields within the same region, assuming that other vent fields are in equilibrium ($x_j=K_j$). A negative dependency of recruitment on population size x_i is introduced as,

$$\left(1-\frac{x_i}{K_i}\right),$$

following the standard formulation of ecological systems limited by a carrying capacity. Here, we assumed that K_i is determined by the total amount of resource supply in vent field i. Our model does not include the duration of pelagic larval phase as a parameter because it is included in the calculation of A (O'Connor et al. 2007, Mitarai et al. 2016). We assumed that x_i is the population size of a species or group of species that share the same niche in vent field i. The species or group of species is assumed to distribute across all vent fields in the same region (connected by dispersal) with sufficient abundance. This assumption is realistic because vent communities frequently have a dominant taxon that constitutes most of the biomass at a regional scale, although the dominance-diversity relationships may depend on environmental conditions such as fluid-flux intensity and sediment types (Portail et al. 2015). Amongst different regions however, it would be reasonable to interpret x_i as the abundance of different species or group of species that accounts for a similar proportion of biomass and having the same growth and dispersal characteristics. We do not directly consider the effect of disturbances on biological diversity because our model accounts for only one species. However, we expect that recoverability of these representative species would be a proxy for the recoverability of other infrequent community members, thus we regarded it as the recoverability of the community as a whole. For example, this is supported by observations of recovery after eruptions (Tunnicliffe et al. 1997, Shank et al. 1998, Marcus et al. 2009, Gollner et al. 2015, Gollner et al. 2017) which showed a concurrence of recovery in total organism density and species richness. While we used the simplest model for our analysis, availability of more detailed data sets that include, for example, biomass, age structure or trophic interactions, would make more extensive models like those used for fishery stock assessments (Walters 1997) applicable and may provide more detailed insights.

2.3. Numerical experiment

Using equation (1,2), we conducted a numerical experiment to calculate the recovery time of HVFs (Fig. 2). We defined the recovery time of a vent field as the time required for the vent field to recover 75% of its original abundance (equal to the carrying capacity of the disturbed vent field by definition) after it was temporarily reduced to zero. We assumed that the carrying capacity is constant throughout time. Our results may underestimate recovery time if population size is highly constrained by the amount of suitable habitat that increases slowly along with the re-establishment of vent fields after disturbances. However, we focused on the resilience of HVFs depending only on the larval supply as this has the strongest influence on recoverability (Lutz et al. 1984).
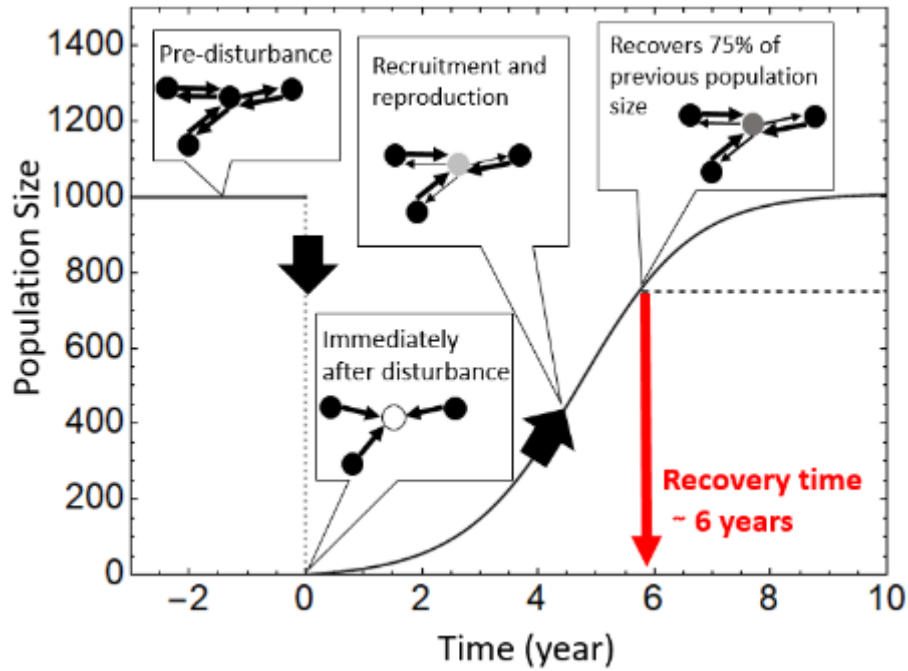
Fig. 2. Schematic distribution of a numerical experiment to estimate recovery time.

2.4. Recovery time for disturbance on multiple HVFs

We evaluated recovery time for disturbance on multiple HVFs as τ_C, where C={X, Y,...} is a possible combination of disturbed HVFs in a region. The procedure to calculate recovery time is the same as previous analyses except population abundance in HVFs included in C were simultaneously reduced to zero. τ_C is the largest recovery time of HVFs included in C, i.e., $\tau_c = \max(\{\tau_i\}_{X \in C})$.

2.5. Optimization

We defined a schedule of resource development, i.e., disturbances, as a vector T={Tx}, where Tx ($X \in \{A, B, C, ...\}$) specifies the timing at which X is disturbed. We used simulated annealing (Box 2; Kirkpatrick et al. 1983) to find the optimal schedule for resource development that can minimize the recovery time. Simulated annealing is a probabilistic technique for approximating the global optimum of a given function. Specifically, it is a metaheuristic approach to approximate global optimization in a large search space. In the algorithm, p(t) is the time dependent acceptance rate of a new schedule when it does not improve the fitting result. This acceptance of worse parameters helps the algorithm find global minima by searching globally at the early stage but locally at the later stage. We assumed that at least one of the Tx is 0 which is the starting point of the disturbances. If Tx >0, X is disturbed after Tx year from the first disturbance. We defined recovery time as the time interval between the first disturbance to 75% recovery of the HVF that is disturbed last.

<div style="border:1px solid orange;">

Box 2. Simulated annealing

1. Set iteration step t=0, set the initial T as a vector whose elements are assigned by a uniform distribution (0,20). Adjust T so that its minimum value is 0 (set T as $T - \min(T)$).
2. Calculate the recovery time τ_C with T.
3. Increment t by 1.
4. Generate a new schedule $T^*=T+\lambda$, where λ is a vector whose elements are assigned by a uniform distribution (-1, 1). Adjust T^* so that its minimum value is 0 (set T^* as $T^* - \min(T^*)$).
5. Calculate the recovery time τ_C^* with T^*.
6. If $\tau_C^* < \tau_C$, or $\tau_C^* \geq \tau_C$ and $rand < p(t)$, set $T=T^*$ and $\tau_C=\tau_C^*$. Here, $rand$ is a random value drawn from a uniform distribution (0,1). p(t) is the acceptance rate of a new parameter vector when it does not improve the fitting result and is $p(t) = \exp(-(\tau_c^* - \tau_c)/\alpha^t)$. Here, we set α=0.99.
7. Back to 4 if t<t_{max}, else terminate the algorithm.

</div>

Example results

3.1. Recovery time

A dispersal matrix of HVFs around Japan is shown in Table 1. The dispersal matrix includes seven HVFs in Okinawa region (Iheya Ridge, Irabu Knoll, Izena Cauldron, Natsushima 84-1 Knoll, North Knoll Iheya Ridge, Dai-Yon Yonaguni Knoll and Hatoma Knoll).

Table 1. Dispersal matrix of HVFs around Japan. Units are larvae/adults/year.

	Iheya Ridge	Irabu Knoll	Izena Cauldron	Natsushima 84-1 Knoll	North Knoll Iheya Ridge	Dai-Yon Yonaguni Knoll	Hatoma Knoll
Iheya Ridge	0.0023	0.0023	0.0053	0.0024	0.0014	0.0006	0.0010
Irabu Knoll	0	0.0067	0	0	0	0.0063	0.0086
Izena Cauldron	0.0030	0.0015	0.0080	0.0038	0.0014	0.0003	0.0008
Natsushima 84-1 Knoll	0.0032	0.0020	0.0076	0.0040	0.0015	0.0003	0.0005
North Knoll Iheya Ridge	0.0037	0.0016	0.0046	0.0023	0.0018	0.0005	0.0006
Dai-Yon Yonaguni Knoll	0	0.0043	0	0	0.0002	0.0050	0.0037
Hatoma Knoll	0	0.0061	0	0	0.0001	0.0068	0.0086

By using this matrix as the dispersal matrix in equation (1,2), we estimated the recovery time (τi) of HVFs in Okinawa and Izu-Bonin region as in Figure 2, Table 2 and 3, respectively. τi in Okinawa was between 3.6 (Natsushima 84-1 Knoll) to 6.1 years (Dai-Yon Yonaguni Knoll).
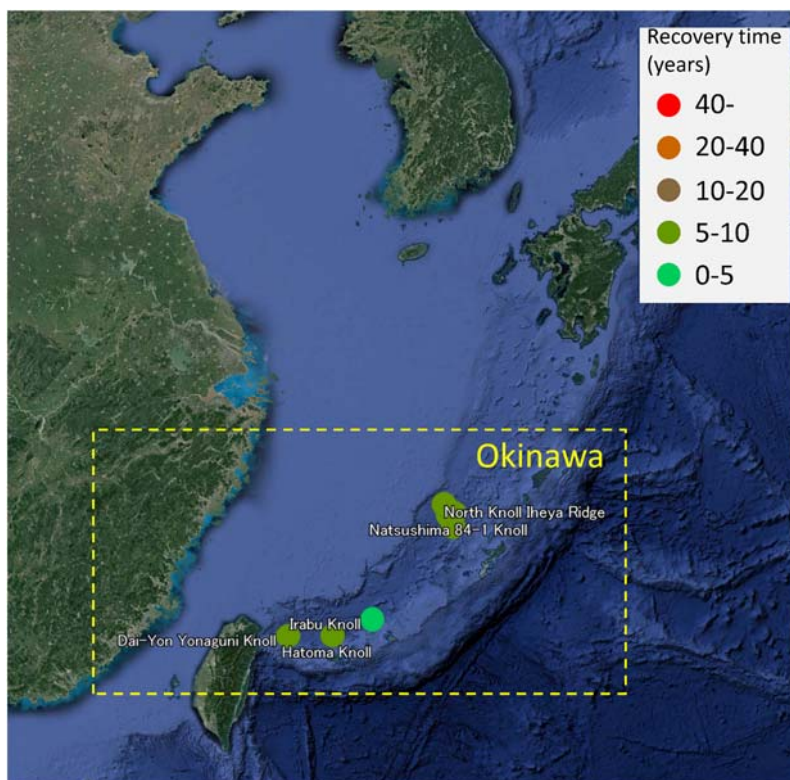
Figure 2. Hydrothermal vent fields around Japan. The map was generated from digital information available at Google Earth Pro v7.3.0.3832 (https://www.google.com/intl/en/earth/; Map data: Google Earth, Image Landsat/Copernicus, Data SIO, NOAA, U.S. Navy, NGA, GEBCO).

Table 2. Recovery time of HVFs in Okinawa shown with other basic properties. Following Suzuki et al. (2018), we set r=17.4 to calculate recovery time. Here, "In-degree" is the number of incoming links, "Self-recruitment" is A_{ii} and "Recruitment from other HVFs" is the sum of A_{ij} (j≠i).

HVFs	τ_i (*years*)	95% CI of τ_i	In degree	Self recruitment (*larvae/adults/year*)	Recruitment from other HVFs (*larvae/adults/year*)
Iheya Ridge	4	0.5 28.9	6	0.0023	0.0130
Irabu Knoll	3.9	0.4 18.9	2	0.0067	0.0149
Izena Cauldron	4.1	0.7 18.7	6	0.0080	0.0107
Natsushima 84-1 Knoll	3.5	0.4 19.1	6	0.0040	0.0152
North Knoll Iheya Ridge	4.3	0.5 32.4	6	0.0018	0.0132
Dai-Yon Yonaguni Knoll	6.2	0.8 30.1	3	0.0050	0.0083
Hatoma Knoll	4.25	0.5 18.6	3	0.0086	0.0130

3.2. Disturbance to multiple HVFs

On-going development of deep-sea resource mining technologies raises the possibility that natural and anthropogenic factors will simultaneously disturb multiple HVFs in a region. Thus, it is worth

evaluating the resilience when multiple HVFs are disturbed.

   In figure 3, recovery time of disturbance to a combination of HVFs (τ_C) is shown as a function of the number of simultaneously disturbed HVFs. For simplicity, we did not consider variation of K in this analysis and assumed K=1,000 for all HVFs. The mean recovery time steadily increases with the number of disturbed HVFs. We found that some combinations substantially delay the recovery as compared to the others. For example, when more than three HVFs were disturbed in Okinawa, τ_C was larger than 20 years if Hatoma Knoll, Dai-Yon Yonaguni Knoll and Irabu Knoll were included in the disturbance, whereas recovery times of other combinations were less than 10 years. In Figure 4, this observation is illustrated by the appearance of the first point showing a recovery time greater than 20 years when three HVFs are simultaneously disturbed. The dispersal matrix for this region (Table 1) shows that if all three HVFs are disturbed, recovery will depend on dispersal from Iheya Ridge to Hatoma Knoll and Dai-Yon Yonaguni Knoll, and dispersal via these links is more than 10 times smaller than the mean dispersal between vents in this region. Further investigation on this observation would benefit by incorporating network analysis, e.g. use of centrality measure (Watson et al. 2011) to distinguish source and sink HVFs, and would provide relevant insight for the application of our approach to management strategy planning.
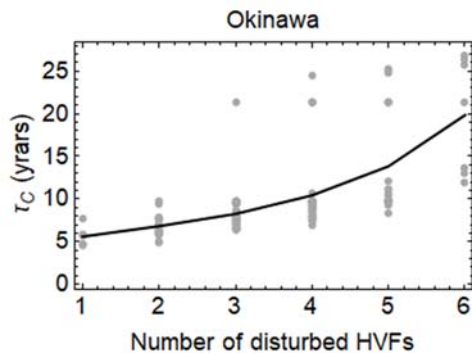
Figure 4. Result of simultaneous disturbances to multiple vent fields for Okinawa. To calculate τ_C, we set r=17.4. Points in figure show τ_C of a combination of HVFs and lines indicate the mean.

3.3.   Optimal scheduling

There were combinations of HVFs that significantly delay recovery, for example, Irabu Knoll, Dai-Yon Yonaguni Knoll and Hatoma Knoll (here we call Irabu, Yonaguni and Hatoma for simplicity) in Okinawa region. In the previous result, we assumed that these HVFs are simultaneously disturbed. However, if the causes of disturbances are anthropogenic factors, such as resource mining, it should be possible to schedule the sequence of mining and interval of disturbances. The recovery time would be minimized if the sequence and interval of disturbances is optimally scheduled. Here, using the disturbance to Irabu, Yonaguni and Hatoma as an example, we show a procedure for optimal scheduling.

Here, the schedule ***T*** is,
$$\boldsymbol{T} = \{T_{Irabu}, T_{Yonaguni}, T_{Hatoma}\},$$

   In this example, the optimal schedule obtained by the simulated annealing (see 2.5) was {1.4, 0, 4.5}, and the recovery time (τ_C, C={Irabu, Hatoma, Yonaguni}) was reduced to 11.3 years, which is about one half the recovery rate when these vents are simultaneously disturbed (21.6 years) (Figure 5). Thus, if the set of targets for resource mining is given, (for example, based on the amount of mineral resources required) the scheduling algorithm could find an optimal schedule to minimize the recovery time.
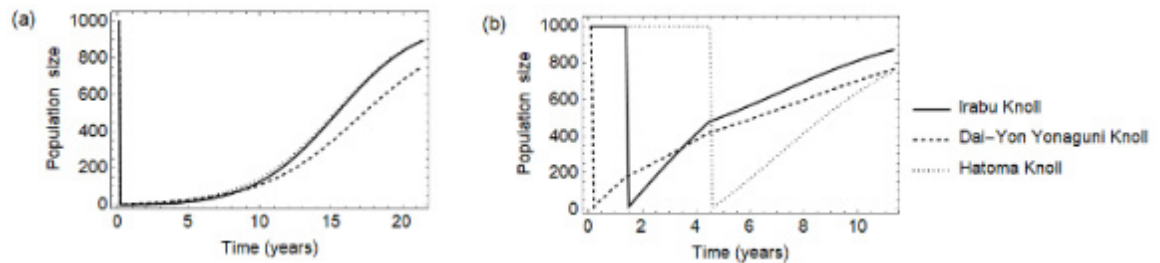
Figure 5. Recovery of population size in the three HVFs with simultaneous disturbances (a) and scheduled disturbances (b).

Software

The following tutorial is presented with interactive python codes on a Jupyter notebook file. Here, we explain how to setup the environment for data analysis on a PC.

4.1. Files

Please download the following files to test the codes or modify it for your own analysis:

1) HowToMapResilienceDemo.ipynb (Jupyter notebook file):
https://drive.google.com/open?id=1dnQGNuSUOmh8jwubOz9-cxeYkkuSLTO4

2) sampledata_okinawa.csv (sample data file):
https://drive.google.com/open?id=1dnr7hvG7SY8zMGP-K5C8xEfo0g3mML6q

and place them in the startup folder of Anaconda (explained later).

4.2. Jupyter notebook

Jupyter notebook is an open-source web application that allows you to run codes and see the output on your internet browser. Jupyter notebook is automatically set up by installing Anaconda. Please install Anaconda with Python 3.X. The installer can be downloaded from the following URL:
https://www.anaconda.com/download/

Please follow the installation guide below:
http://docs.anaconda.com/anaconda/install/

Please see following document for how to launch Jupyter notebook:
http://docs.anaconda.com/anaconda/user-guide/getting-started/

If you succeed in launching Jupyter notebook, you will find a new tab on your default internet browser showing contents in the startup folder of Anaconda. Please open "HowToMapResilienceDemo.ipynb" to test the codes or use it for your own analysis. If you cannot find the file, please move it to the startup folder and refresh the tab.

Tutorial for the data analysis

5.1. Data import

The first step is to load the python modules (a set of functions) and data file. To run the codes, place the cursor somewhere in the cell and push "Shift+Enter".

```
In [3]: %matplotlib inline
        import pandas as pd
        import numpy as np
        import copy
        import matplotlib.pyplot as plt
        import itertools

        data = pd.read_csv("./sampledata_okinawa.csv",sep=",",header=0)
        hvfnames=list(np.array(data.T)[0])
        nhvfs=len(hvfnames)
        dispersalMatrix=np.array(data.as_matrix())[:,1:]
```

Here, "*sampledata_okinawa.csv*" is a CSV file for the dispersal matrix. The file path must be altered when applying the following analysis to a different dataset (*NOTE: This is only a procedure required to apply the following analysis to your dataset if you do not need to change other parameters*). Please be sure that each element in the matrix represents recruitment of larvae from a HVF j (row) to i (column), and the first column and rows must be the name of the HVFs (see 2.1).

The following code shows a dispersal matrix:

```
In [4]: pd.DataFrame(dispersalMatrix,index=hvfnames,columns=hvfnames)
Out[4]:
```

	Iheya Ridge	Irabu Knoll	Izena Cauldron	Natsushima 84-1 Knoll	North Knoll Iheya Ridge	SPOT Dai-Yon Yonaguni Knoll	SPOT Hatoma Knoll
Iheya Ridge	0.002281	0.00234	0.005349	0.002376	0.001407	0.000567	0.000994
Irabu Knoll	0	0.006708	0	0	0	0.006281	0.008571
Izena Cauldron	0.003016	0.001548	0.008017	0.003775	0.001366	0.000275	0.000756
Natsushima 84-1 Knoll	0.003174	0.001994	0.007631	0.003973	0.001512	0.000345	0.000507
North Knoll Iheya Ridge	0.003676	0.001555	0.004608	0.002347	0.001805	0.000479	0.000568
SPOT Dai-Yon Yonaguni Knoll	0	0.004336	0	0	0.00021	0.004978	0.003714
SPOT Hatoma Knoll	0	0.0061	0	0	0.000131	0.006814	0.0086

5.2. Recovery time for a fixed K value

The following codes define a function that numerically integrates the differential equation (1, 2), by Euler method ("*populationDynamics*") and a function that returns recovery time based on the numerical solution of the equation ("*recoverytime*"). We set "*thr*" as 0.75 since we defined recovery as the time required for x_{i} to recover 75% of its original abundance after it was temporarily reduced to zero. This value must be changed if readers use another definition for the recovery time.

```
In [13]:  thr=0.75

          def populationDynamics(x0,aii,sumkaij,k,r,dt):
              xi=x0+(aii*x0*r+r*sumkaij)*(1-x0/k)*dt
              return xi

          def recoverytime(pid,dispersalMatrix,k,r):
              t=0
              ais=list(copy.deepcopy(dispersalMatrix[pid]))
              aii=ais[pid]
              del ais[pid]
              aij=ais
              sumkaij=k*sum(aij)
              xi=0
              Xi=[xi]
              dt=0.1
              while t<10000 and xi<thr*k:
                  t=t+1
                  xi=populationDynamics(xi,aii,sumkaij,k,r,dt)
                  Xi.append(xi)
              rt=len(Xi)*dt
              return rt
```

The following codes show a table with the recovery time of each HVF under a fixed value of carrying capacity "*k=1000*" and reproduction rate "*r=17.4*". The value of "*r*" might be changed if readers identified species-specific values for reproduction rate, i.e., mean number of larvae that one individual produces per year.

```
In [196]:  k=1000
           r=17.4

           vrectime=[]
           for i in range(7):
               rt=recoverytime(i,dispersalMatrix,k,r)
               vrectime.append(rt)

           pd.DataFrame(vrectime,index=hvfnames,columns=["Recovery time (years)"])
```

Out[196]:

	Recovery time (years)
Iheya Ridge	5.8
Irabu Knoll	4.6
Izena Cauldron	5.7
Natsushima 84-1 Knoll	4.8
North Knoll Iheya Ridge	5.8
SPOT Dai-Yon Yonaguni Knoll	7.7
SPOT Hatoma Knoll	4.8

5.3. Recovery time for the ensemble of various spatial distribution of K values

Variability of recovery time can be evaluated by assuming variation in K values. The following function should be used to calculate recovery time for the ensemble of K values generated from a probability distribution.

```
In [129]:  def recoverytimeRnd(pid,dispersalMatrix,ks,r,dt):
              t=0
              ais=copy.deepcopy(list(dispersalMatrix[pid]))
              aii=ais[pid]
              del ais[pid]
              aij=ais
              ki=copy.deepcopy(ks[pid])
              del ks[pid]
              kjs=ks
              sumkjaij=np.dot(aij,kjs)
              xi=0
              Xi=[xi]
              while t<10000 and xi<0.75*ki:
                  t=t+1
                  xi=populationDynamics(xi,aii,sumkjaij,ki,r,dt)
                  Xi.append(xi)
              rt=len(Xi)*dt
              return rt
```

In the following codes, we calculated recovery time of each HVF for 1,000 random distributions of K values. Here, K values are assigned from a log-normal distribution with mean 1,000 and s.d. 1.

```
In [132]:  lognormal_mean=1000
           lognormal_sd=1
           it=1000
           r=17.4

           RTS=[]
           for i in range(nhvfs):
               i=i+1
               rts=[]
               for i in range(it):
                   dt=0.1
                   mdks=list(np.random.lognormal(np.log(lognormal_mean), lognormal_sd, nhvfs))
                   rt=recoverytimeRnd(0,dispersalMatrix,mdks,r,dt)
                   rts.append(rt)
               RTS.append(rts)
```

The following codes show the summary statistics of the recovery time of HVFs for the ensemble of K values:

```
In [133]:  pds=pd.DataFrame(np.array(RTS).T,columns=hvfnames)
           pds.describe()
```

Out [133]:

	Iheya Ridge	Irabu Knoll	Izena Cauldron	Natsushima 84-1 Knoll	North Knoll Iheya Ridge	SPOT Dai-Yon Yonaguni Knoll	SPOT Hatoma Knoll
count	1000.000000	1000.00000	1000.000000	1000.00000	1000.000000	1000.000000	1000.000000
mean	6.554600	6.75640	7.014500	6.49160	6.371000	6.488000	6.651100
std	7.284511	8.03996	7.608164	6.77281	7.041048	7.474427	7.277033
min	0.200000	0.20000	0.200000	0.20000	0.200000	0.200000	0.200000
25%	1.900000	2.00000	2.200000	2.00000	1.900000	1.900000	2.000000
50%	4.100000	4.20000	4.400000	4.30000	4.100000	3.900000	4.100000
75%	8.500000	8.40000	8.900000	8.50000	8.100000	8.100000	8.600000
max	52.900000	64.70000	58.100000	57.70000	56.900000	66.100000	61.100000

5.4.   Disturbance to multiple HVFs

The final task is to calculate the recovery time when multiple HVFs are disturbed. Here, we defined the combination of disturbed HVFs as C and recovery time is the largest recovery time of HVFs included in C. In this example, C consists of indices from 0 to 6 and each index corresponds to Iheya Ridge, Irabu Knoll, Izena Cauldron, Natsushima 84-1 Knoll, North Knoll Iheya Ridge, Dai-Yon Yonaguni Knoll and Hatoma Knoll, respectively. Thus, "[0,2,4]" stands for "[Iheya Ridge, Izena Cauldron, North Knoll Iheya Ridge]". For simplicity, we did not consider variation of K in this analysis and assumed a constant carrying capacity "$k=1000$" for all HVFs, i.e., we focused on the effect of disturbances on the mean recovery time.

The following function provides the numerical solution of the population dynamics in all HVFs

simultaneously by solving a differential equation whose variable is a vector:

```
In [83]: def populationDynamicsMulti(xs,dispersalMatrix,ks,r,dt):
             xi=xs+(r*np.dot(dispersalMatrix,xs))*(1-xs/ks)*dt
             return xi
```

The following function returns largest recovery time of HVFs included in C:

```
In [3]: def recoverytimeMulti(C,dispersalMatrix,r):
            ks=np.array([1000 for i in range(nhvfs)])
            xs=copy.deepcopy(ks)
            for i in C:
                xs[i] = 0
            t=0
            dt=0.1
            xi=xs
            Xi=[xi]
            while t<1000 and np.min(xi/ks)<0.75:
                t=t+1
                xi=populationDynamicsMulti(xi,dispersalMatrix,ks,r,dt)
                Xi.append(xi)
            rt=len(Xi)*dt
            return rt
```

The following codes generate all possible combinations of disturbance (C) and calculates recovery time. The number of combinations that include the same number of HVFs are [7, 21, 35, 35, 21, 7].

```
In [134]: r=17.4
          hvfindices=range(0,nhvfs)
          rtss=[]
          for j in range(1,nhvfs):
              delcombi=list(itertools.combinations(hvfindices, j))
              rts=[]
              for listx in delcombi:
                  rt=recoverytimeMulti(listx,dispersalMatrix,r)
                  rts.append(rt)
              rtss.append(rts)
```

The following codes show the recovery time (points), mean recovery time (line) and the 95%CI (colored area) as a function of the number of HVFs included in C:

```
In [224]: rtmean=list(map(lambda x: np.mean(x), rtss))
          rtqup=list(map(lambda x: np.percentile(x,97.5), rtss))
          rtqdw=list(map(lambda x: np.percentile(x,2.5), rtss))
          x=list(range(1,nhvfs))

          xi=0
          splx=[]
          sply=[]
          for y in rtss:
              xi = xi +1
              for yi in y:
                  splx.append(xi)
                  sply.append(yi)

          #plot
          plt.xlabel('Number of disturbed vent fields', fontsize=18)
          plt.ylabel('Recovery time (years)', fontsize=18)
          plt.plot(x, rtmean)
          plt.fill_between(x, rtqup, rtqdw, alpha=.25)
          plt.scatter(splx,sply)
          #legend(loc=' lower right' , fontsize=18)
```

Out[224]: <matplotlib.collections.PathCollection at 0x1e4f1f38358>
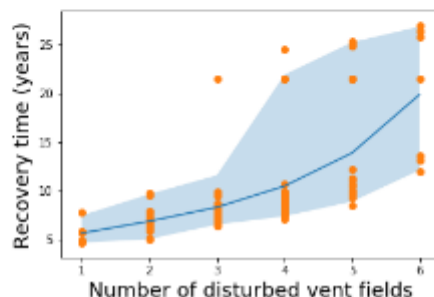
5.5. Optimal scheduling

The final task is to find the optimal schedule *T* when multiple HVFs are disturbed.

The following function returns recovery time for a give set of HVFs *C* and schedule *T*:

```
In [260]: def recoverytimeMultiSch(C,dispersalMatrix,r,T):
              ks=np.array([10000 for i in range(nhvfs)])
              xs=copy.deepcopy(ks)
              lenc=len(C)
              dt=0.1
              t=0
              count=0
              for i in range(lenc):
                  if abs(T[i]/dt - t) < 0.99:
                      xs[C[i]] = 0
                      count=count+1
              xi=xs
              Xi=[xi]
              while (t<10000 and np.min(xi/ks)<0.75) or count != lenc:
                  t=t+1
                  for i in range(lenc):
                      if abs(T[i]/dt - t) < 0.99:
                          xi[C[i]] = 0
                          count=count+1
                  xi=populationDynamicsMulti(xi,dispersalMatrix,ks,r,dt)
                  Xi.append(xi)
              rt=len(Xi)*dt
              return rt
```

The following code shows that recovery time of simultaneous disturbance to Irabu Knoll (1), Hatoma Knoll (5) and Dai-Yon Yonaguni Knoll (6) is 21.4 years:

```
In [267]: r=17.4
          recoverytimeMultiSch([1,5,6],dispersalMatrix,r,[0,0,0])
Out[267]: 21.400000000000002
```

The following codes define functions for optimal scheduling using a simulated annealing:

```
In [287]: exp = math.e
          alpha = 0.99

          def prob(e1, e2, t):
              if e1 > e2:
                  return 1
              else:
                  return exp**((e1-e2)/t)

          def temperature(t):
              return alpha**t

          def optimalSchedule(C,dispersalMatrix,r):
              le=len(C)
              T=list(randint(0,100,le)*0.1)
              T=list(T-min(T))
              rt=1000
              t=0
              while(t<1000):
                  t=t+1
                  nT = [x + y for (x, y) in zip(T, list(randint(-10,10,le)*0.1))]
                  nT =list(nT-min(nT))
                  nrt=recoverytimeMultiSch(C,dispersalMatrix,r,nT)
                  if nrt<rt or rand() < prob(rt, nrt, temperature(t)):
                      rt=nrt
                      T=nT
              return rt, T
```

The following code shows that the recovery time can be reduced to 11.1 years if *T* is optimally scheduled:

```
In [293]: r=17.4
          optimalSchedule([1,5,6],dispersalMatrix,r)
Out[293]: (11.100000000000001, [4.800000000000006, 0.0, 0.30000000000000249])
```

Limitations and future works

Our analysis can be applied to different regions if the dispersal matrix between HVFs is obtained. Addition of newly found HVFs can be done by simply adding new rows and columns to the previous matrix. In future studies, researchers should attempt to reveal dispersal networks in a broader region of the world ocean, with a wider range of taxonomic and habitat types, which will extend the coverage of this analysis. This will allow us to map the resilience of different species, allowing comparative studies on the relationship between resilience and species traits. However, presented results were obtained by omitting various biological details. Information about biological traits (e.g., larval development, ontogenetic vertical migration, and settling behaviors) is essential to accurately predict larval dispersal distance and species-specific resilience. Furthermore, we did not consider the activity and configuration of individual vents in each HVF. HVFs may include both active and inactive vent systems. In this study, we focused on the recoverability of communities in active vent systems. Our results can be applied to chemosynthetic communities in inactive vent systems, if they are included in or located close to the HVFs included in the analysis. However, because of the limited resource supply, recoverability of inactive vent systems could be lower than active vent systems (Gollner et al. 2017). It is important to integrate information regarding the detailed spatial structure and the predictions obtained by fine scale physical modelling, such as the local fluid-flux and amount of sedimentation caused by resource mining, to accurately predict the relationship between disturbances and recovery time at more detailed spatial scales.

It also should be mentioned that there is still a relative lack of empirical data from disturbance-recovery studies that can support our results. All previous studies have been carried out on either the Juan De Fuca Ridge (Tunnicliffe et al. 1997, Marcus et al. 2009) or the East Pacific Rise (Shank et al. 1998, Gollner et al. 2015). Because both are in a fast spreading ridge where biological communities are frequently disturbed (e.g., ~ 15 years [Tolstoy et al. 2006]), it would be controversial whether these results represent recovery of HVFs in slow spreading ridges or arc-backarc basins where disturbance to communities are relatively infrequent (Gollner et al. 2017). However, our results still suggest substantial differences in recovery time among HVFs, which can span two orders of magnitude, highlighting the importance of understanding connectivity among HVFs to assess their recoverability (Suzuki et al. 2018).

References

Beerli P, Palczewski M (2010) Unified framework to evaluate panmixia and migration direction among multiple sampling locations. Genetics 185: 313-326.

Binns RA, Scott SD (1993) Actively forming polymetallic sulfide deposits associated with felsic volcanic rocks in the eastern Manus back-arc basin, Papua New Guinea. Econ Geol 88: 2226-2236.

Chen C, Copley JT, Linse K et al (2015) Low connectivity between 'scaly-foot gastropod' (Mollusca: Peltospiridae) populations at hydrothermal vents on the Southwest Indian Ridge and the Central Indian Ridge. *Org Divers Evol* 15: 663-670.

Coffey Natural Systems (2008b) Environmental Impact Statement. Solwara 1 project. Nautilus Minerals Niugini Limited, Main Report. Coffey Natural Systems. Brisbane.

D'Arcy R, Amend JP, Osburn MR (2013) Microbial diversity and potential for arsenic and iron biogeochemical cycling at an arsenic rich, shallow-sea hydrothermal vent (Tutum Bay, Papua New Guinea). Chem Geol 348: 37-47.

Desbruyères D, Hashimoto J, Fabri M-C (2006) Composition and biogeography of hydrothermal vent communities in western Pacific back-arc basins. In: Christie DM, Fisher CR, Lee, S-M et al (ed) Back-Arc Spreading Systems: Geological, Biological, Chemical, and Physical Interactions. American Geophysical Union, Washington D. C., p 215-234.

Gollner S, Govenar B, Arbizu PM et al (2015) Differences in recovery between deep-sea hydrothermal vent and vent-proximate communities after a volcanic eruption. Deep Sea Res I 106: 167-182.

Gollner S, Kaiser S, Menzel L et al (2017) Resilience of benthic deep-sea fauna to mining activities. Mar Environ Res 129: 76-101.

Grassle JF (1986) The ecology of deep-sea hydrothermal vent communities. Adv Mar Biol 23: 301e362.

Grassle JF, Sanders H(1973) Life histories and the role of disturbance. Deep Sea Res 20: 643e659.

Halbach P, Nakamura KI, Wahsner M et al (1989) Probable modern analogue of Kuroko-type massive sulphide deposits in the Okinawa Trough back-arc basin. Nature 338: 496-499.

Herzig PM (1999) Economic potential of sea–floor massive sulphide deposits: ancient and modern. Phil Trans R Soc Lond A 357, 861-875.

Hoagland P, Beaulieu S, Tivey MA (2010) Deep-sea mining of seafloor massive sulfides. Mar Policy 34: 728-732.

Holling CS (1973) Resilience and stability of ecological systems. Annu Rev Ecol Syst 4: 1-23.

Holling CS (1996) Engineering resilience versus ecological resilience.In: National Academy of Engineering (ed) Engineering within ecological constraints. National Academies Press, Washington DC, p 31-44.

Ives AR, Carpenter SR (2007) Stability and diversity of ecosystems. Science 317: 58-62.

International Seabed Authority (2007)Polymetallicsulphides and cobalt‑rich ferromanganese crusts   deposits: establishment ofenvironmentalbaselines andanassociatedmonitoringprogrammeduringexploration, https://www.isa.org.jm/files/documents/EN/Workshops/2004/Proceedings-ae.pdf.

Jannasch HW, Wirsen CO (1979) Chemosynthetic primary production at East Pacific sea floor spreading centers. Bioscience 29: 592-598.

Jeanthon C (2000) Molecular ecology of hydrothermal vent microbial communities. Antonie Leeuwenhoek 77: 117-133.

Kirkpatrick S, Gelatt CD, Vecchi MP (1983) Optimization by simulated annealing. Science 220: 671-680.

Le JT, Levin LA, Carson RT (2016) Incorporating ecosystem services into environmental management of deep-seabed mining. Deep Sea Res II, 137: 486-503.

Levin LA, Baco AR, Bowden DA et al (2016) Hydrothermal vents and methane seeps: rethinking the sphere of influence. Front Mar Sci 3: 72.

Lutz RA, Jablonski D, Turner RD (1984). Larval development and dispersal at deep-sea hydrothermal vents. Science 226: 1451-1454.

Macdonald K, Becker K, Spiess FN et al(1980) Hydrothermal heat flux of the 'black smoker' vents on the East Pacific Rise. Earth Planet Sci Lett 48: 1e7.

Mahon BP, Bhatt A, Vullo D et al (2015) Exploration of anionic inhibition of the α-carbonic anhydrase from *Thiomicrospira crunogena* XCL-2 gammaproteobacterium: a potential bio-catalytic agent for industrial CO_2 removal. Chem Engi Sci 138: 575-580.

Marcus J, Tunnicliffe V, Butterfield DA (2009) Post-eruption succession of macrofaunal communities at diffuse flow hydrothermal vents on Axial Volcano, Juan de Fuca Ridge, Northeast Pacific. Deep Sea Res II 56: 1586-1598.

Mitarai S et al (2016) Quantifying dispersal from hydrothermal vent fields in the western Pacific Ocean. Proc Nat Acad Sci 113: 2976-2981.

O'Connor MI, Bruno JF, Gaines SD et al(2007) Temperature control of larval dispersal and the implications for marine ecology, evolution, and conservation. Proc Nat Acad Sci 104: 1266–1271.

Podowski EL, Ma S, Luther, GWIII et al (2010) Biotic and abiotic factors affecting distributions of megafauna in diffuse flow on andesite and basalt along the Eastern Lau Spreading Center, Tonga. Mar Ecol Prog Ser 418: 25-45.

Portail M, Olu K, Escobar-Briones E(2015)Comparative study of vent and seep macrofaunal communities in the Guaymas Basin. Biogeosci 12: 5455-5479.

Shank TM, Fornari DJ, Von Damm KL et al(1998)Temporal and spatial patterns of biological community development at nascent deep-sea hydrothermal vents (9 50` N, East Pacific Rise). Deep Sea Res II 45:465-515.

Suzuki K, Yoshida K, Watanabe H et al (2018) Mapping the resilience of chemosynthetic communities in hydrothermal vent fields. *Sci Rep* 8: 9364.

Terpe K (2013) Overview of thermostable DNA polymerases for classical PCR applications: from molecular and biochemical fundamentals to commercial systems. Appl Microb Biotech 97: 10243-10254.

Tolstoy M, Cowen JP, Baker ET et al(2006)A sea-floor spreading event captured by seismometers. Science 314: 1920-1922.

Tunnicliffe V, Embley RW, Holden JF et al (1997) Biological colonization of new hydrothermal vents following an eruption on Juan de Fuca Ridge. Deep Sea Res I 44: 1627-1644.

Van Dover CL (2014) Impacts of anthropogenic disturbances at deep-sea hydrothermal vent ecosystems: a review. Mar Environ Res 102: 59-72.

Walters C, Christensen V, Pauly D (1997) Structuring dynamic models of exploited ecosystems from trophic mass-balance assessments. Rev Fish Biol Fisher 7: 139-172.

Watanabe H, Fujikura K, Kojima S et al(2010) Japan: Vents and seeps in close proximity.In: Kiel S (ed) The Vent and Seep Biota, Springer, Dordrecht, p 379–402.

Watson JR, Siegel DA, Bruce EK et al (2011) Identifying critical regions in small-world marine metapopulations. Proc Nat Acad Sci 108: 907-913.

SIP Protocol Series

SIP Protocol No.1

Application of environmental metagenomic analyses for environmental impact assessments

SIP Protocol No.2

Genetic Connectivity Survey Manuals

SIP Protocol No.3

A rapid method to analyze meiofaunal assemblages using an Imaging Flow Cytometer

SIP Protocol No.4

Acquisition of Long-Term Monitoring Images Near the Deep Seafloor by Edokko Mark I

SIP Protocol No.5

Microstructure Measurements aroud Deep Sea floor
-Direct Measurements of the Deep Sea Turbulence flow-

SIP Protocol No.6

Onboard bioassay for seawater quality monitoring using delayed fluorescence of microalgae

SIP Protocol No.7

How to map the resilience of hydrothermal vent fields: a tutorial

Contact

Dr. Masanobu Kawachi
National Institute for Environmental Studies (NIES)
16-2 Onogawa, Tsukuba, 305-8506 JAPAN

TEL +81-29-850-2345   FAX +81-29-850-2587
E-mail kawachi.masanobu@nies.go.jp